Supporting Material:
Lipid Mediated Packing of Transmembrane Helices - A Dissipative Particle Dynamics Study

Ayelet Benjamini
Department of Chemistry,
University of California in Berkeley, Berkeley, CA

Berend Smit
Department of Chemistry,
University of California in Berkeley, Berkeley, CA
Department of Chemical and Biomolecular Engineering,
University of California in Berkeley, Berkeley, CA
Materials Sciences Division,
Lawrence Berkeley National Laboratory, Berkeley, CA

Box-and-Whisker diagrams

In Figures 5, 6(a) and S2 we use a box-and-whisker diagram to represent the distribution of angles (cross and projection angles). In constructing these box-and-whisker diagrams we follow Frigge *et al.*[1]. The diagrams represent five important statistics of a distribution:

(1) The median (Q_2), represented by a thick horizontal line.

(2) The lower (Q_1) and upper (Q_3) quartiles, represented by the lower and upper edges of the box, respectively.

(3) The lowest data point within 1.5 IQR of the lower quartile and the highest data point within 1.5 IQR of the upper quartile, represented by the lower and upper whiskers, respectively. IQR = $(Q_3 - Q_1)$ is the interquartile range.

This representation allows for an easy comparison between large sets of distributions.

Potential of Mean Force Calculations

In this work we obtain the potential of mean force (PMF) between several helix pairs. To that end we use the traditional umbrella sampling method[2] with a heavy-harmonic biasing potential. That is, we split the entire examined range into overlapping windows specified by a range (ξ_1, ξ_2). The biasing potential for each window corresponds to:

$$U_{bias}(\xi) = \begin{cases} \frac{1}{2}K(\xi - \xi_1)^2 & \xi < \xi_1 \\ 0 & \xi_1 \leq \xi \leq \xi_2 \\ \frac{1}{2}K(\xi - \xi_2)^2 & \xi > \xi_2 \end{cases} \tag{1}$$

Since we sample in the $NP_\perp \gamma T$ ensemble, in which the area constantly changes, we preform umbrella sampling in scaled units, *i.e.* $\xi = r/L_x$ where $L_x = L_y$ is the instantaneous box-size along the plane of the membrane and r is the inter-helical distance. We simulate ξ values ranging from $\xi_{min} = 0.035$ up to $\xi_{max} = 0.5$ in windows of size $\Delta\xi = 0.006$. For some helix pairs, containing super positive mismatched helices, a smaller $\xi_{min} = 0.029$ is used, as these helices tend to approach closer to one another. In real units this roughly corresponds to range (8 Å, 120 Å) with windows of size ~ 1.5 Å. The biasing potential constant is set to $K \simeq 50.0\ \varepsilon_0/d_0^2 = 78500\ \varepsilon_0/[\xi]^2$. We simulate the system in each window for 20000 cycles. We then un-bias and combine the results of each window using the weighted histogram analysis method (WHAM)[3] to obtain the PMF. We normalize the results to account for the metric jacobian. We reiterate this procedure by adding the inverse of the PMF we obtained in the previous iteration to the biasing potential, until we obtain uniform sampling throughout the entire range. Finally we convert the scaled ξ coordinates to the reduced units by multiplying over by the average box-size: $r = \xi \cdot \langle L_x \rangle$. Results for the Potential of Mean Force of all helix pairs, including error bars, are provided in Fig. S5.

Importance of Helicity

This work explores the cross angle distribution of TM helices and finds that these are very close to the cross angle distribution of two vectors with pre-determined tilt angle distributions. It is therefore tempting to model TM helices as simple rods (or cylinders), and not resolve their helical nature. Yet this approach yields a non realistic configuration of packed peptides.

Non-Charged Cylinders   We explored the cross angles of a cylindrical model identical to what is described by de Meyer *et al.*[4]. The peptide is modeled by seven bonded chains, each containing n_{tp} hydrophobic beads at the core and 3 hydrophilic beads at each end. The radius of the cylinder is 6.8Å which corresponds to the radius of an α-helix and to the radius of our CG helical model. This cylindrical model of TM peptides was shown to produce realistic tilt angles[5] and a PMF similar in trends to the one observed here[4,6].

We have sampled the cross angle in homogeneous pairs of cylinders. The results for cross angle distribution in pairs of $n_{tp} = 4, 5, 8, 9$ and 10 are presented in Fig. S2. These chain lengths correspond to hydrophobic mismatch $\Delta d = -10.0$Å, -5.5Å, 8.0Å, 12.6Å and 17.1Å, respectively. Pairs of $n_{tp} = 6, 7$ ($\Delta d = -1.0$Å, 3.5Å) did not stay in a packed configuration and are therefore not presented. The results show that in all hydrophobic mismatches considered, the mean cross angle distribution was smaller than that of the helical model, averaging on only $\langle \Omega \rangle \sim 14.7°$. This behavior is in contrary to the cross angles typically observed in natural helices[7], where $\langle \Omega \rangle \sim 32°$ and can reach as high as $\Omega = 120°$. The cylinders tend to adopt a tight parallel configuration and not cross. Typical packed configurations are presented in Fig. S3(a),S3(b).

Charged Cylinders   We expected the existence of a permanent dipole moment in α-helices to support a crossed configuration of the peptides, rather than a parallel one[8]. We therefore further modified the cylinder model to include partial charges. These charges were chosen to mimic the dipole moment in α-helices, which is a result of all carbonyl groups pointing in the direction of the helix major axis. To that end we added partial charges to beads in the cylindrical model (see Fig. S3(c)). In DPD, soft repulsive forces are applied between the CG beads. There is therefore no explicit hard core interaction and special care needs to be taken when applying electrostatic forces to avoid divergence at zero distances. We followed the method developed by Groot[9] for adding electrostatics in DPD simulations, and use a smeared-out charge in the center of charged beads.

As we were interested in exploring the local effect of charges on the packing of a pair of peptides, we made some simplifications in our simulation. We applied charges only on a small set of beads along the surface of the cylinder model. We did not model charges on other system components such as water and lipid head groups as these are accounted for explicitly in the un-bonded interaction parameters of those beads[5]. Additionally, we did not account for interaction with the nearest image as we focused on the local interaction of peptides. We therefore calculated the force resulting in electrostatic interactions explicitly by adding the short range contribution. Furthermore, we have assumed that all charges interact through the hydrophobic membrane medium (dielectric constant $\varepsilon = 2$ as per Groot[9]), and not screened through the water medium. This assumption represents the extreme case of stronger electrostatic interactions. Based on these simplifications, we are hesitant to say that this model captures the full effect of partial charges along the surface of the peptide. However, we do believe that we have captured the first-order effect of such charges and we don't expect our results to change qualitatively had we done more extensive changes.

We added partial charges along the surface of the cylinder model, in a helical manner (see Fig. S3(c)).

The charges were added such that the total dipole of 0.5 electron charge [10,11] is spread out along the surface of the helix. We sampled the cross angle distribution of homogenous pairs of charged cylinders with $n_{tp} = 5, 6, 8, 9$ and 10. Charged cylinders with $n_{tp} = 4, 7$ did not remain in packed configurations and were therefore not accounted for in cross angle distribution calculations.

Results for these simulations are presented by the blue filled box-and-whisker diagrams in Fig. S2. Even in the presence of partial charges the configuration of paired peptides remained roughly parallel. We observe a slight increase in the average cross angle to $\langle \Omega \rangle \sim 15.6°$, but cross angle values were still much lower than typical cross angles in natural TM helices. The configuration remained parallel, shifting the peptide surface such that positively partially charged beads of one peptide faced the negatively partially charged beads of the paired peptide.

Comparison to All-Atoms

To test the validity of our bonded interaction parameters, we compared the fluctuation in our model helix's length to that of a natural helix, simulated in a membrane environment using all atoms simulations. To that end we use the helix structure 1SPF, provided in the RCSB database [12]. We inserted the helix to a pre-equilibrated bilayer of DPPC lipids and preformed initial equilibration using the CHARMM-GUI program [13]. We then simulated the membrane embedded helix for a total of 5ns in the $NP_\perp \gamma T$ ensemble, and obtain a histogram of its natural length fluctuations. Ensemble parameters were chosen to match those in our CG simulation. These fluctuations in helix length were then compared to the length fluctuations of a CG helix of similar size (containing 27 residues). Results are presented in Fig. S4.

We do not expect a perfect match between these distributions, for several reasons: 1. These are not identical helices; 2. The nature of CG models is such that finer structural details cannot be resolved, and so wider fluctuations are expected; and finally 3. The helix simulated in all-atom simulations included hydrophilic residues only on one end, while the CG model contains hydrophilic residues on both ends. Different driving forces for stretching and shrinking are therefore expected. Despite all these differences, we see a reasonable agreement in the distribution of helix length, with more flexibility in the CG helix model. The all-atoms helix length corresponds to $H_L^{AA} = 35.7\text{Å} \pm 0.54\text{Å}$, while the coarse grained helix length corresponds to $H_L^{CG} = 34.2\text{Å} \pm 0.71\text{Å}$. In Fig. S4 we present the deviations around the mean helix length for easier comparison.

Sampling

In order to avoid correlations between helix pairs configurations, we sample each helix pair system over 30 different copies. We are interested only in sampling packed configurations. We therefore initialize the position of helices to be close to each other (~ 3.5 nm), such that dimerization occurs fast. The helices are also free to distant themselves from one another and configurations of non-packed helices are also observed. We sample cross angles only from time frames in which the helices are in contact (see main text).

We make sure sampling is sufficient in each system copy by observing sufficient fluctuations around a mean value throughout the simulation. We present an example for the time evolution of cross angles in three different system copies in Fig. S6. These were obtain from helices with negative $(-9\text{Å}, -9\text{Å})$ mismatch. In these copies helices remained in contact through most of the simulation time.
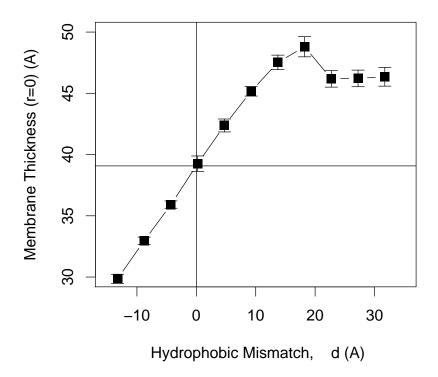
Figure S1

Figure 1 Membrane thickness (d_M) around a single TM helix. Thickness was calculated based on the positions of the second head-group bead in the lipid model, in both top and bottom leaflets. This is equivalent to calculating the membrane Phosphorous-to-Phosphorous distance. Filled squares represent extrapolated membrane thickness at zero distance ($r = 0$) from the helix. Whiskers represent one standard deviation in thickness. The unperturbed membrane thickness (d_M^0) is represented by the solid horizontal line at 39.1Å. These results show that the membrane thickness at $r = 0$ is roughly linearly increasing with hydrophobic mismatch. A change in this trend is apparent for super-positive mismatched helices, where the membrane thickness reaches a plateau of $d_M = 46.25\text{Å} \pm 0.09\text{Å}$. This value corresponds to $d_M^0 + 7.2\text{Å}$.
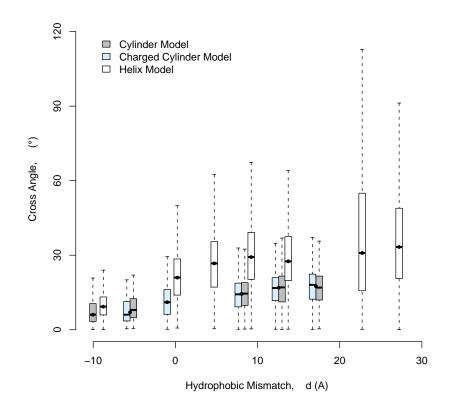
Figure S2

Figure 2 Cross angle distribution of homogenous TM peptides as a function of hydrophobic mismatch. Only packed configurations (inter-peptide distance < 15Å) were considered. Filled box-and-whisker diagrams represent the cross angle distribution in the cylinder model of de Meyer *et al.*[4], with (blue) and without (grey) partial charges. Empty box-and-whisker diagrams represent the cross angle distribution in the helix model presented in this work. Black points represent the hydrophobic mismatch for each box-and-whisker diagrams. Charged and uncharged cylinder model have identical hydrophobic mismatch.

Figure S3

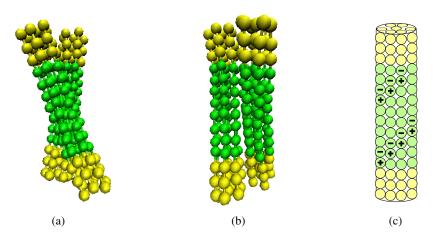(a)   (b)   (c)

Figure 3 Cylinder model of TM peptide. (a) and (b) Show a typical crossed configuration of cylinder model peptides from front and side view, respectively. A crossed configuration of cylinder peptides presents a much lower cross angle than that of helical peptides, as can be seen in Fig. S2. (c) Shows the distribution of charges along the surface of a cylinder model.
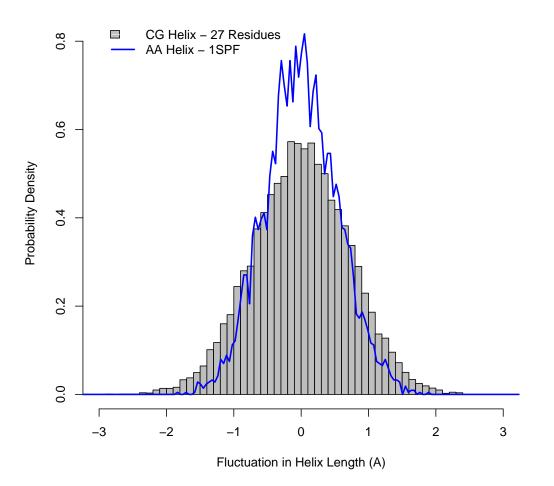
7

Figure 4 Comparison of helix length distribution of a model coarse grained (CG) helix of 27 residues (grey boxes) and a helix structure from the PDB database (1SPF), simulated with all-atoms (AA) simulation technique (blue line). The histograms are aligned around the mean value of each simulated helix, which correspond to $H_L^{AA} = 35.7$Å for the all-atom helix and $H_L^{CG} = 34.2$Å for the coarse grained helix. These distributions show the fluctuations in helix length in both simulation techniques are substantial. The CG model captures fairly well the inherent fluctuations in helix length, showing a tendency towards a broader distribution.

Figure 5 Potential of Mean Force for helix pairs. Each helix pair is displayed in a separate plot with the according error bars. The hydrophobic mismatch values of the helices in the pair are displayed in units of $(\text{Å}, \text{Å})$ in the legend of each plot.

Figure 6 Time evolution of cross angles as sampled in three different copies of a system with negative $(-9\text{Å}, -9\text{Å})$ mismatched helices. The helices remained in contact through most of these frames. The time evolutions shows no significant biases with respect to time, suggesting sufficient sampling.

Table S1

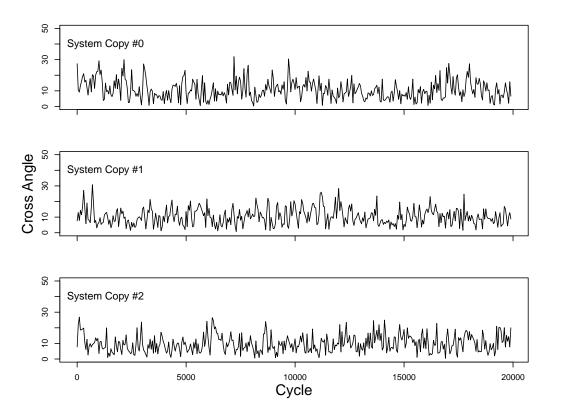| Interaction	Interacting Beads			Force constant	Equilibrium value
U_{bond}				$K_b\ (\varepsilon_0/d_0{}^2)$	$r_{eq}\ (d_0)$
	P_i	S_{i-1}		100	0.7936
	P_i	S_i		100	0.7936
	P_i	P_{i+4}		100	1.1241
	C_k	C_{k+1}		100	0.6960
	C_k	P_{3k}		20	0.9575
	C_k	P_{3k+1}		20	0.9290
	C_k	P_{3k+2}		20	0.9575
U_{angle}				$K_a\ (\varepsilon_0/rad^2)$	$\varphi_{eq}\ (°)$
	P_i	P_{i+1}	P_{i+2}	600	81.2
	P_i	P_{i+4}	P_{i+5}	100	108.9
	C_k	C_{k+1}	C_{k+2}	20	180.0
$U_{dihedral}$				$K_d\ (\varepsilon_0)$	$\chi_{eq}\ (°)$
	P_i	P_{i+1}	P_{i+2} P_{i+3}	1000	21.7

Table 1 Bonded interaction parameters in the coarse-grained TM helix model. Interaction energies are calculated as described in Eq. 1 in the main text.

Table S2

Pair	Mismatch (Å)	Single $\langle\theta\rangle$ (°)	Single σ_θ (°)	Pair $\langle\theta\rangle$ (°)	z-value	Z-Score
(-13,-9)	-13.27	11.19	5.89	11.19	0.00	
	-8.77	9.47	4.93	9.08	-0.08	-0.04
(-9,-9)	-8.77	9.47	4.93	8.98	-0.10	
	-8.77	9.47	4.93	8.95	-0.11	-0.10
(0,0)	0.23	16.66	6.72	15.96	-0.10	
	0.23	16.66	6.72	15.78	-0.13	-0.12
(5,5)	4.73	19.99	7.61	19.55	-0.06	
	4.73	19.99	7.61	19.69	-0.04	-0.05
(5,9)	4.73	19.99	7.61	19.34	-0.09	
	9.23	25.66	7.28	24.55	-0.15	-0.12
(5,14)	4.73	19.99	7.61	19.20	-0.10	
	13.73	30.84	7.97	29.31	-0.19	-0.15
(9,9)	9.23	25.66	7.28	22.27	-0.47	
	9.23	25.66	7.28	22.06	-0.49	-0.48
(9,14)	9.23	25.66	7.28	20.61	-0.69	
	13.73	30.84	7.97	24.55	-0.79	-0.74
(9,18)	9.23	25.66	7.28	20.19	-0.75	
	18.23	32.97	7.18	31.19	-0.25	-0.50
(14,23)	13.73	30.84	7.97	20.28	-1.32	
	22.73	48.27	4.69	42.61	-1.21	-1.27
(18,23)	18.23	32.97	7.18	24.59	-1.17	
	22.73	48.27	4.69	38.09	-2.17	-1.67
(23,23)	22.73	48.27	4.69	39.22	-1.93	
	22.73	48.27	4.69	39.45	-1.88	-1.90
(27,27)	27.23	52.96	4.51	47.58	-1.19	
	27.23	52.96	4.51	47.54	-1.20	-1.20

Table 2 Tilt angles of interacting helices. For each pair in Fig. 6 of the main text, we compare the helix average tilt angle when paired to another helix (Pair $\langle\theta\rangle \equiv \langle\theta\rangle^P$) to the helix average and standard deviation in tilt angle when isolated in the membrane (Single $\langle\theta\rangle \equiv \langle\theta\rangle^S$, Single $\sigma_\theta \equiv \sigma_\theta^P$, respectively). Based on the single helix distribution of tilt angles, we calculate the z-value of the observed mean tilt angle in the paired configuration $(z_i = \frac{\langle\theta_i\rangle^P - \langle\theta_i\rangle^S}{\sigma_{\theta_i}^S}, i = 1, 2)$. We then obtain the scaled mean distance of the pair, $Z = \frac{1}{2}(z_1 + z_2)$. This Z-Score provides a measurement of how likely is it, in units of standard deviation, that the tilt angles of helices in a pair were obtained from the single helix tilt angle distribution. Pair configurations where the tilt angle of each helix remains the same as when isolated correspond to small absolute value Z-score. Pair configurations where the tilt angle of each helix differs greatly from the single helix configuration correspond to large absolute value Z-score.

Table S3

PDB	Chain	Residue Range	Length (Å)	Mismatch (Å)
2jln	A	296 : 329	51.64	21.04
3kcu	A	247 : 278	50.89	20.19
2bl2	B	90 : 122	56.43	20.03
2bl2	D	90 : 122	57.14	20.74
2bl2	G	90 : 122	56.04	19.64
2bl2	H	90 : 122	55.90	19.50
2xq2	A	348 : 380	49.89	19.29
1ots	A	33 : 69	56.39	25.89
1ots	B	33 : 69	56.22	25.72
2iqv	A	120 : 152	56.15	23.45
2a65	A	89 : 124	54.76	24.16
2a65	B	89 : 124	54.76	24.16
3hqk	A	83 : 113	52.32	21.72
3din	D	30 : 64	51.71	24.01
1kpl	A	32 : 66	57.08	26.98
1kpl	B	33 : 67	53.14	23.04
3org	A	90 : 127	58.54	29.04
3org	D	90 : 127	58.53	29.03
2wsx	A	35 : 70	50.14	20.74
2wsx	C	35 : 70	50.11	20.71
2wsx	B	35 : 70	49.93	20.53

Table 3 Natural super-positive mismatched helices. Natural helices with hydrophobic mismatch greater than 19Å are described by the PDB entry and chain they are present in, at a certain residue range. Helix hydrophobic length and hydrophobic mismatch are calculated following the analysis in Benjamini *et al.*[7].

References

[1] M. Frigge, D. C. Hoaglin and B. Iglewicz, *American Statistician*, 1989, **43**, 50–54.

[2] G. M. Torrie and J. P. Valleau, *Journal of Computational Physics*, 1977, **23**, 187–199.

[3] S. Kumar, D. Bouzida, R. Swendsen, P. Kollman and J. Rosenberg, *Journal of Computational Chemistry*, 1992, **13**, 1011–1021.

[4] F. J.-M. de Meyer, M. Venturoli and B. Smit, *Biophysical Journal*, 2008, **95**, 1851–1865.

[5] M. Venturoli, B. Smit and M. M. Sperotto, *Biophysical Journal*, 2005, **88**, 1778–1798.

[6] K. Bohinc, V. Kralj-Iglic and S. May, *Journal of Chemical Physics*, 2003, **119**, 7435–7444.

[7] A. Benjamini and B. Smit, *Biophysical Journal*, 2012, **103**, 1227–1235.

[8] W. G. J. Hol, *Progress in Biophysics & Molecular Biology*, 1985, **45**, 149–195.

[9] R. D. Groot, *Journal of Chemical Physics*, 2003, **118**, 11265–11277.

[10] A. Wada, *Advances in Biophysics*, 1976, **9**, 1 – 63.

[11] D. Sengupta, R. N. Behera, J. C. Smith and G. M. Ullmann, *Structure*, 2005, **13**, 849–855.

[12] *Research Collaboratory for Structural Bioinformatics (RCSB) Protein Data Bank*, `http://www.rcsb.org`.

[13] S. Jo, T. Kim, V. G. Iyer and W. Im, *Journal of Computational Chemistry*, 2008, **29**, 1859 – 1865.